Structure and performance of clay composite membranes with improved sodium conductivity for salinity gradient batteries

Applied Clay Science 245 (2023) 107136

Contents lists available at ScienceDirect

Applied Clay Science

journal homepage: www.elsevier.com/locate/clay

Research Paper

Structure and performance of clay composite membranes with improved sodium conductivity for salinity gradient batteries

Nadia Boulif, Renate Evers, Menno Houben, Zandrie Borneman, Kitty Nijmeijer *

Membrane Materials and Processes, Department of Chemical Engineering and Chemistry, Eindhoven University of Technology, P.O. Box 513, 5600 MB Eindhoven, the Netherlands

ARTICLE INFO

Keywords:
Cation exchange membrane
Montmorillonite clay
Composite
Salinity gradient battery

ABSTRACT

Low-cost cation exchange membranes with improved ionic conductivity and permselectivity are needed for the deployment of efficient large-scale energy storage technologies or separation technologies such as electrodialysis. In this work, a series of montmorillonite (Mt) clays and sulfonated poly(ether ether ketone) (SPEEK) composite membranes with 1 to 20 weight percentage (wt%) additives are studied. Two types of clays are investigated, a generic K30 Mt and an aluminum pillared (Al-pil) Mt with larger interlayer spacing owing to the inorganic crosslinks between the clay platelets. The addition of inorganic clays with two-dimensional geometries enables the formation of percolating sodium diffusing pathways with reduced tortuosity. As a result, the conductivity of the membranes increases with an increasing clay loading fraction, reaching up to 1.4 times that of the pure SPEEK with 20 wt% K30 Mt. The permselectivity of the native SPEEK membrane also improves with the addition of set amounts of K30 Mt, while the Al-pil Mt composites suffer from a slightly reduced permselectivity due to their higher water uptake. The voltaic efficiency of a concentration gradient flow battery shows that the addition of 20 wt% K30 Mt clay to the SPEEK polymer matrix can improve the voltaic efficiency by up to 10%.

1. Introduction

Salinity gradient flow batteries are an attractive approach for energy storage: they use non-toxic, abundant and safe materials (sodium chloride and water), and they are easy to scale up thanks to a decoupled energy storage and power output (van Egmond et al., 2016). These aqueous redox flow batteries use the processes of electrodialysis and reverse electrodialysis to store and retrieve electrical energy in the form of a chemical potential. During the battery charge, the electrical energy is used to create a chemical potential gradient by increasing the concentration difference between two solutions. During the battery discharge, the stored chemical potential is converted back to electrical energy by reverse electrodialysis (Nijmeijer and Metz, 2010; Guler and Nijmeijer, 2018). To achieve 100% energy storage efficiency, the membranes contained in a salinity gradient battery should ideally have no resistance (to minimize the ohmic energy losses) and 100% permselectivity to achieve the highest potential (Nijmeijer and Metz, 2010; van Egmond et al., 2016; Guler and Nijmeijer, 2018).

Still, the technology is currently limited by, among others, the lack of ion exchange membranes (IEMs) that combine both high permselectivity and high conductivity (Güler et al., 2013; Fan and Yip, 2019). Currently, most commercially available IEMs consist of a randomly arranged ion exchange polymer matrix which sometimes contains a reinforcing material (Sarapulova et al., 2019). As a result of their lack of molecular organization, the ionic diffusion pathways in IEMs are tortuous, resulting in ionic diffusion coefficients that are 10 to 100 times lower than in solution (Guggenheim, 1954; Kingsbury et al., 2018; Sarapulova et al., 2019). This causes the membranes to have poor conductivities.

Presently, the best commercially available membranes in terms of conductivities are those based on state-of-the-art perfluorinated polymers such as Nafion (Kreuer, 2001; Abbasi et al., 2021). The high performance of these membranes is attributed to their ability to form highly segregated hydrophobic domains (that prevent undesired water transport) and highly interconnected hydrophilic domains through which the transport of cations occurs (Kreuer, 2001; Hugo et al., 2018; Abbasi et al., 2021). However, these materials are expensive and their use in the European Union is threatened by possible future legislation regarding the ban of perfluorinated materials due to safety and environmental concerns (Ghasemi et al., 2013; Hugo, 2020; National Institute for Public Health and the Environment, 2023). Therefore, there have been

* Corresponding author.
E-mail address: d.c.nijmeijer@tue.nl (K. Nijmeijer).

https://doi.org/10.1016/j.clay.2023.107136
Received 27 June 2023; Received in revised form 7 September 2023; Accepted 8 September 2023
Available online 23 September 2023

increasing efforts in the past years to achieve similar or better-performing membranes based on cheaper and more environmentally friendly materials (Gaowen and Zhentao, 2005; Güler et al., 2013; Fan and Yip, 2019).

The addition of an inorganic material to a polymeric matrix is a facile way to combine the singular properties of the fillers with a cheap hydrocarbon material (Krishnan et al., 2006; Namdari et al., 2017). Particularly, the addition of fillers with a one-dimensional (1D) or two-dimensional (2D) morphology is of interest to reduce the tortuosity of the ionic transport pathway, thereby increasing the effective diffusion coefficient inside the membrane (Radmanesh et al., 2019). For example, Fan et al. (2020) showed that the addition of sulfonated carbon nanotubes to a sulfonated poly(ether ether ketone) (SPEEK) membrane improves the membrane conductivity by creating straight percolating pathways without impairing the membrane permselectivity (Fan et al., 2020). Nonetheless, carbon nanotubes are expensive and their handling is challenging (Bhattacharya, 2016).

Another source of abundant and cheap high aspect ratio additives are smectite clays such as montmorillonite (Mt), which typically have a 2D platelet morphology (Król-Morkisz and Pielichowska, 2019; Zhou et al., 2019; Massaro et al., 2020). Due to the presence of silanol groups that become negatively charged when in contact with water, clays are especially interesting additives for cation exchange membranes (CEMs) as they have intrinsic cation exchange capacity on their surface (Li et al., 2017). These properties make Mt a potential candidate to locally shorten the sodium diffusion pathway in the membrane by making it straighter; therefore, improving the membrane conductivity. Molecular dynamics simulations have shown that the sodium ion diffusion coefficient in the clay interlayer is roughly a fourth of that of sodium in bulk water, and even higher for ions in hydrated clays (Bourg and Sposito, 2010; Greathouse et al., 2016). Previous works have already looked into the addition of montmorillonite clay into a SPEEK matrix. However, these studies mainly focused on the addition of clay to improve the membrane barrier properties for methanol fuel cells rather than improving the conductivity (Gosalawit et al., 2008; Doğan et al., 2011; Charradi et al., 2019). Therefore, their focus was on creating perfectly exfoliated composites and the surface of the clays was modified by means of a compatibilizer, rendering the clays non-contributing to the ionic diffusion in the membrane (Chang et al., 2003; Gaowen and Zhentao, 2005; Lee et al., 2007). However, to the best of the author's knowledge, no study so far has reported the use of non-compatibilized clays in composite membranes, which takes advantage of the naturally occurring diffusion highways within the Mt clay to improve a membrane's conductivity.

In this work, we aim to investigate the effect of the non-compatibilized clay loading on the membrane ionic conductivity and selectivity to study the effect of the addition of naturally abundant 2D cationic exchange materials on the membrane performance. The polymer matrix chosen was a SPEEK polymer as it is currently considered to be one of the promising and cheaper alternatives to Nafion (Ghasemi et al., 2013; Hugo, 2020; Abbasi et al., 2021). Furthermore, Güler et al. have shown that the best power density of a reverse electrodialysis stack was obtained when using lab-made SPEEK cation exchange membranes (Güler et al., 2013). To this polymer matrix, two types of clays were added: a K30 Mt, which is an acid-treated natural clay, and an aluminum pillared clay (Al-pil Mt) in which the different platelets are crosslinked with inorganic aluminum oxide pillars (Flessner et al., 2001; Tepmatee and Siriphannon, 2013). The K30 Mt can form exfoliated, intercalated, and microcomposite structures while the Al-pil Mt can only form the intercalated and microcomposite structures since the inorganic crosslinks prevent the exfoliation of the platelets (Müller et al., 2017). This study aims to investigate whether the two different types of clays will interact differently with the polymer matrix, and therefore lead to different microcomposite structures. The effect of the composite type and structure is correlated to the membrane charge density, ionic conductivity, permselectivity and performance in a salinity gradient flow battery.

2. Materials and methods

2.1. Materials

Sulfonated poly(ether ether ketone) (SPEEK) (Fumion® E-670, ion exchange capacity (IEC) = 1.565 meq/g, sulfonation degree: 52%, Lot P1311–175) was purchased in the form of fibers from FumaTech-BWT GmbH (Germany). The K30 montmorillonite (K-catalyst, 330 m^2/g, pH 2.8–3.8) and the aluminum pillared montmorillonite (surface area: 250 m^2/g, pH 4–5, loss on ignition: 12–19%) were bought from Sigma-Aldrich (Germany). *N*-methyl pyrrolidone (NMP, industrial grade) was acquired from ViVoChem B.V. (The Netherlands). Sodium chloride (NaCl, Sanal® P, pharmaceutical quality) was kindly supplied by Nouryon (The Netherlands). For the membrane characterization, 1 M hydrochloric acid (HCl, Supelco® from Sigma Aldrich, Germany), sodium sulfate decahydrate (Na_2SO_4, >99%, Acros Organics, Spain), potassium chloride (KCl, ACS reagent, 99.0–100.5%, Merck, Germany) and sodium hydroxide (NaOH, > 99%, VWR Chemicals, Czech Republic) were used. Iron (III) chloride hexahydrate (puriss. p.a., ≥ 99%) and iron (II) chloride tetrahydrate (puriss. p.a., ≥ 99.0%) were purchased from Sigma-Aldrich (Germany) and were used to prepare the electrolyte for the concentration gradient flow batteries. The demineralized water was obtained from an Elga Water Purification System from Veolia (The Netherlands). All chemicals were used as received.

2.2. Membrane preparation

Composite membranes with 1, 5, 10, 15, and 20 wt% K30 Mt or Al-pil Mt (based on the SPEEK weight) were prepared as follows and as depicted in Fig. S1 (see supplementary information).

The desired amount of clay was sonicated at room temperature in 20 mL NMP for one hour using a Branson 3510 Ultrasonic Bath (Marshal Scientific, United States). 5 g of SPEEK polymer fibers were then added and the solutions were left overnight on a roller bench (LABINCO rolling bench from Labinco BV, The Netherlands, set on stand 2). Just before casting, the solutions were again sonicated for one hour. The solutions were cast on a glass plate using a 500 μm casting knife, after which they were dried for two days in a nitrogen box and six days in a nitrogen oven (universal oven from Memmert GmbH + Co. KG, Germany) at 120°C. The free-standing membranes were recovered from the glass plate and were immersed in water for three days to remove possible solvent residues. The obtained dense membranes were then stored in 0.5 M NaCl.

2.3. Membrane characterization

2.3.1. Water uptake

The water uptake was determined in triplo for each membrane type by immersing the rinsed membrane samples (3 × 3 cm^2) in demineralized water for at least 48 h. They were then carefully wiped with paper to remove excess solution and weighed. After that, the samples were put in a vacuum oven (Memmert GmbH + Co. KG, Germany) at 60°C for 24 h. The samples were weighed again and the water uptake (WU, in wt%) was determined using the following equation:

$$WU = \frac{m_{wet} - m_{dry}}{m_{dry}} \bullet 100\% \quad (1)$$

where m_{wet} is the weight of the wet membrane (g) and m_{dry} is the dried membrane's weight (g).

2.3.2. Ion exchange capacity

The ion exchange capacity of the membranes was determined in duplicates using an acid-base titration as reported in previous works (Güler et al., 2013). First, the membrane samples (3 × 3 cm^2) were immersed overnight in 1 M HCl to bring the membrane into H^+-form. They were then thoroughly rinsed with demineralized water and soaked

for one hour in demineralized water to remove the residual sorbed protons from the membrane surface. The water was frequently refreshed. The samples were then immersed in 50 mL 3 M NaCl solution for three hours to displace the H^+ out of the membrane and into the solution. Each hour, the salt solution was refreshed. For each membrane sample, the combined salt solutions were titrated with 0.1 M NaOH using a titrator (Compact titrator G20 from Metler Toledo (United States), equipped with a DGi115-SC electrode). The membrane samples were then dried in a vacuum oven at 60°C for 24 h.

The ion exchange capacity (IEC) (meq/g dry membrane, equivalent in S.I. units to moles of fixed charges/kg dry membrane) was then determined using Eq. (2):

$$\mathrm{IEC} = \frac{M_{\mathrm{NaOH}} \bullet V_{\mathrm{NaOH}}}{m_{\mathrm{dry}}} \tag{2}$$

where M_{NaOH} is the concentration of the used sodium hydroxide solution (M), V_{NaOH} the volume of sodium hydroxide needed to titrate the acid (mL), and m_{dry} the weight of the dried membrane (g).

The IEC of the clays (for samples of 1 g) was measured in a similar way, except that centrifugation (using a CompactStar CS4 centrifuge from VWR International (Austria) at 6500 rpm for five minutes) was used to recover the clays from the solution and that they were dried in the vacuum oven at 60°C till constant weight.

2.3.3. Membrane permselectivity

The membrane permselectivity was determined using a two-compartment cell as reported in previous works (Güler et al., 2013; Kingsbury and Coronell, 2021). A membrane sample with an exposed area of 17.3 cm^2 was separating two compartments of 131 mL through which 1 L 0.1 and 1 L 0.5 M KCl solution were recirculated with a peristaltic pump (MasterFlex L/S, Cole-Parmer, United States) on each side of the membrane (residence time: 45 s). The open cell voltage was monitored at 25°C over the membrane for an hour with an Ivium n-stat (IVIUM Technologies BV, The Netherlands). Duplicates were measured for each membrane sample, and two samples were used for each membrane type. The membrane permselectivity (α, in %) was determined according to:

$$\alpha = \frac{V_{\mathrm{measured}}}{V_{\mathrm{theoretical}}} \bullet 100\% \tag{3}$$

where V_{measured} is the potential measured across the membrane in the setup (V) and $V_{\mathrm{theoretical}}$ is the theoretically computed potential (V) based on the Nernst equation.

2.3.4. Membrane resistance

The membrane resistance was determined with 0.5 M NaCl at 25°C using a six-compartment cell as mentioned in previous works (Güler et al., 2013). The resistance measurements were carried out using an Ivium n-stat (IVIUM Technologies BV, The Netherlands). Several currents in the ohmic regime of the membranes (from 0 to 1.0 mA/cm^2 in steps of 0.1 mA/cm^2 and 1.5, 2.0 and 2.5 mA/cm^2) were applied and the corresponding voltage drop over the membrane was measured via Haber-Luggin capillaries. The resistance was determined from the slope of the voltage vs. current with a coefficient of determination above 0.999.

The membrane areal resistance was computed according to:

$$R_{\mathrm{areal,membrane}} = (R_{\mathrm{membrane}} - R_{\mathrm{blank}}) \bullet A_{\mathrm{membrane}} \tag{4}$$

where $R_{\mathrm{areal,membrane}}$ is the resistance by the membrane area (Ω.cm^2), R_{membrane} and R_{blank} are the resistances (Ω) measured with the membrane and without the membrane, respectively, and A_{membrane} is the area of the exposed membrane in cm^2.

The membrane conductivity ($\sigma_{\mathrm{membrane}}$ in mS.cm) was computed using the following formula:

$$\sigma_{\mathrm{membrane}} = \frac{t_{\mathrm{membrane,wet}}}{R_{\mathrm{areal,membrane}}} \bullet 10^{-3} \tag{5}$$

where $t_{\mathrm{membrane,wet}}$ is the wet membrane thickness (cm) and $R_{\mathrm{areal,membrane}}$ is the areal resistance membrane (Ω.cm^2).

2.3.5. Thermogravimetric analysis (TGA)

The membrane thermal stability was determined using thermogravimetric analysis (TGA). The measurements were performed using a PerkinElmer TGA 4000 (TA instruments, part of Waters™, United States of America) under an N_2 flow of 40 mL/min and heating from 50 to 900°C at a rate of 20°C/min.

2.3.6. Differential scanning calorimetry (DSC)

The glass transition temperature (T_g) of the polymers was determined by differential scanning calorimetry (DSC) using a TA Instruments DSC Q2000 (TA instruments, part of Waters™, United States of America). Three heating and cooling cycles were performed from −20 to 280°C at a rate of 5°C/min. The T_g was determined from the second cycle using the half-height point method from the TRIOS software from TA instruments.

2.3.7. Scanning electron microscopy (SEM) and elemental analysis with energy dispersive X-ray spectroscopy (EDS)

The morphological analysis of the membranes was performed using a JEOL JSM-IT100 scanning electron microscope (Jeol, The Netherlands). The samples were observed at a 1000 times magnification at a working distance of 10 mm, using an applied voltage of 10.0 kV and a probe current of 50. The cross-section images were obtained by cryogenically fracturing the membrane samples after wetting them in ultrapure water. Before observation under the SEM, the samples were coated with platinum for 60 s at 40 mA using a JEOL JFC-2300 HR sputter coater.

2.3.8. Attenuated total reflection Fourier transform infrared spectroscopy (ATR FT-IR)

The ATR FT-IR spectrum of membrane samples was recorded using a Varian 3100 FT-IR spectrometer (Agilent, United States) equipped with a golden gate attenuated total reflectance (ATR) sampling accessory. The spectra were acquired from 650 to 4000 cm^{-1} using 50 scans per spectrum.

2.3.9. Membrane performance in a concentration gradient battery

The membrane performance was determined in a salinity gradient battery. This battery uses electrodialysis to convert the supplied electrical energy to a concentration gradient (chemical potential gradient). The stored energy is then retrieved by reverse electrodialysis, where the chemical potential is used to spontaneously generate electrical energy, as described by van Egmond et al. (2016). The cell design was similar to that reported by Al-Dhubhani et al. (2021), except that no bipolar membrane was used. Therefore, the CEM separated only two 0.5 M NaCl compartments. The spacers in the concentrate and dilute compartment had a thickness of 3.2 mm and were made by layering a rubber gasket, a 3D printed flow frame, and a rubber gasket. The electrolyte used was a 0.25 M $FeCl_2$, 0.25 M $FeCl_3$, and 0.1 M HCl solution that was circulated at 150 mL/min in both electrolyte compartments. 50 mL of 0.5 M NaCl was recirculated in the concentrate and the dilute compartment at a flow velocity of 1 cm/s. Each membrane was tested for three cycles that consisted of a charge step of 440 mA for one hour and a discharge step of −440 mA for one hour. The measurements were made with a portable SP-300 potentiostat from BioLogic (France). A schematic of the experimental setup can be found in Fig. S2 (see supplementary information).

Before and after each experiment, a blank was measured by having one AEM in between the two electrolyte compartments and applying constant currents from 0 to 450 mA in steps of 50 mA for 30 s. The potential was recorded for each current step and the resistance of the

blank was determined. The voltage measured in the battery cycling experiments was corrected for this blank resistance in order to make the voltaic efficiency results independent of changes in the electrolyte resistance.

The coulombic efficiency (CE) was determined by calculating the ratio of the discharge capacity to that of the charge capacity. The voltaic efficiency (VE) was the ratio of the discharge time-average voltage to that of the charge. The round-trip efficiency was computed from the product of CE and VE.

3. Results and discussion

3.1. Membrane structure and thermal properties

Several composite membranes with K30 Mt and Al-pil Mt were prepared by solution casting. The clays did not fully exfoliate and dissolve in the organic solvent due to the lack of use of compatibilizers to prevent coverage of the clay surface blocking ionic transport. Therefore, above a clay loading of 5 wt%, the number and size of clay aggregates increase. As shown in the SEM and elemental analysis picture (Fig. 1), clay aggregates are not visible in the 1 wt% K30 Mt and 1 wt% Al-pil Mt composite membrane, but start to be formed from 5 wt% on. The Mt is homogeneously distributed in the polymeric matrix, although it tends to sediment towards the bottom of the film during the drying process due to its higher density (2–3 g/cm^3 as reported by Uddin (2018)) than that of the polymer (0.85 to 1.14 g/cm^3 as reported by Mahajan and Ganesan (2010)). As the clay concentration increases above 5 wt%, the size and number of clay aggregates increase and the clay-rich domains span an increasingly larger fraction of the membrane thickness. For the K30 Mt composites, the 10 μm clay aggregates span 36% of the membrane thickness at 5 wt% K30 Mt, while this fraction increases to 47% for the 40 μm K30 Mt aggregate shown in the sample with a clay loading of 20 wt%. The presence of these aggregates that sediment towards the bottom of the membrane surface is not believed to be problematic for the application of these films as membranes, since the clays are incorporated in the film and have an effect on the membrane properties as will be shown below when discussing the obtained results.

The interaction between the clay and the polymer matrix is

Table 1
T_g values of the pure SPEEK membrane and the K30 Mt and Al-pil Mt composite membranes with a clay loading of 1 to 20 wt%.

Weight percent additive (wt%)	Additive type	
	K30 Mt	Al-pil Mt
	T_g (°C)	
0	225	
1	247	220
5	250	206
10	247	203
15	238	208
20	224	220

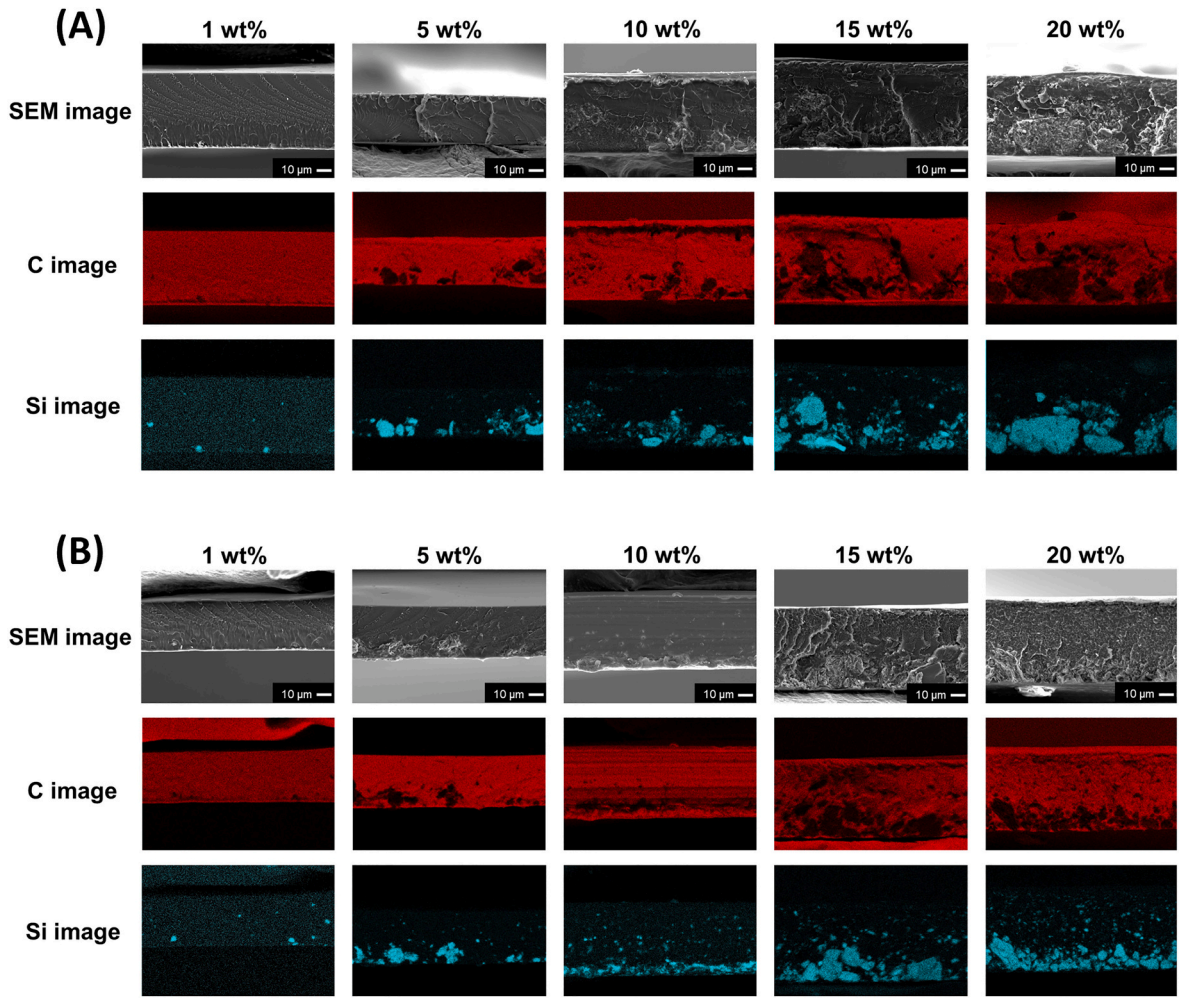

Fig. 1. SEM images and corresponding EDX analysis of the composite membranes cross sections. (A): K30 Mt composites and (B): Al-pi Mt composites. The carbon image is used to map the regions with containing the SPEEK polymer and the silicon for the Mt domains.

investigated by DSC (Table 1), as the addition of nanoparticles can alter the glass transition temperature (T_g) by reducing the polymer chains' mobility at the clay-polymer interface (DeFelice and Lipson, 2021).

In the case of the K30 Mt, the T_g increases by up to 25°C compared to the native SPEEK polymer matrix whereas it decreases by up to 22°C in the case of the Al-pil composites. This is due to the physical interaction between the K30 Mt surface and the polymer chains which locally reduces their mobility, while the larger and fixed interlayer distance between the clay platelets in Al-pil Mt acts as a plasticizer by increasing the distance between the SPEEK chains (see Fig. 2) (Xu et al., 2004). The K30 Mt can (partially) exfoliate, causing the entire surface of clay platelets to become available for interactions with the polymer chains, reducing their mobility. Furthermore, the exfoliated platelets can also fill the free volumes of the polymer matrix, which also contributes to a higher T_g (Muralidharan et al., 2008). On the other hand, the Al-pil Mt can only form intercalated and microcomposite structures due to the inorganic crosslinks between the platelets, which hinder the formation of strong polymer-clay interactions as the availability of free clay surface area is decreased. As a result, the distance between the polymer chains is increased, and their mobility increases. The maximum effect of the clay loadings on the composite T_g is observed at 5 wt% K30 Mt and 10 wt% Al-pil Mt. This suggests that at low clay loading fractions (1 wt%), the amount of clay added is too low to affect to a sufficient extent all the bulk of the polymer matrix. As the clay loading increases above 5 wt% K30 Mt or 10 wt% Al-pil Mt, the size of the clay aggregates increases, which reduces the effective contact area available for polymer-clay interactions.

To better understand this phenomenon, an FT-IR of a pure SPEEK membrane, a 1 wt% K30 Mt-SPEEK composite, and a 1 wt% Al-pil Mt composite were recorded. Fig. 3 shows that the addition of only 1 wt% K30 Mt changes the shapes of the peaks that correspond to the sulfonic acid group (at 1160, 1186, and 1215 cm^{-1}) and the C-O-C stretching at 842 cm^{-1}, while the vibrational stretching of the C═O bond at 1720 cm^{-1} is greatly enhanced (Xing et al., 2004; Shukla and Thakur, 2010; Kumar et al., 2014). The changes in these three functional group vibrational energies support the hypothesis of strong clay-polymer interactions despite the lack of compatibilizer use, which reduces the chain mobility as shown in Table 1 (Shukla and Thakur, 2010). On the other hand, the 1 wt% Al-pil Mt composite FT-IR spectrum shows no difference from that of the native SPEEK membrane, suggesting that there are no strong interactions between the Al-pil Mt and the SPEEK polymer as seen in Table 1.

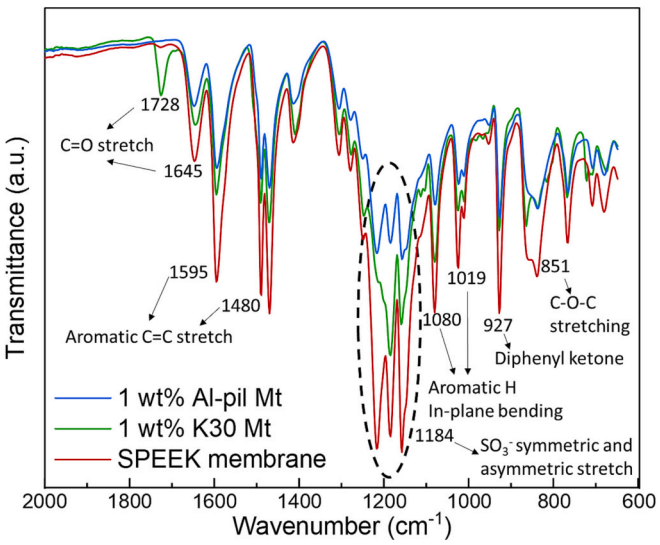

Fig. 3. ATR FT-IR spectra of a pure SPEEK membrane, a 1 wt% K30 Mt composite membrane, and a 1 wt% Al-pil Mt composite membrane. The numbers next to the peaks correspond to the position in reciprocal cm (cm^{-1}) of the peak and the text indicates the corresponding functional group.

The thermal stability of the membranes was further investigated with

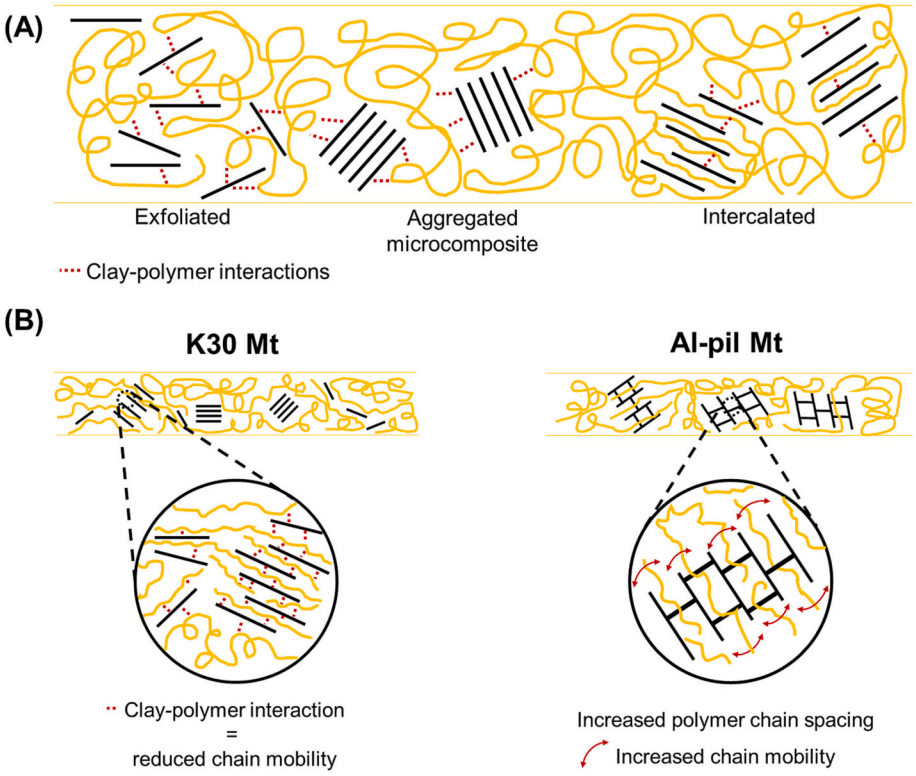

Fig. 2. (A) Different types of composite structures that can be obtained and (B) the difference between K30 Mt composites nanostructure and Al-pil Mt composites nanostructure.

TGA, as shown in Fig. 4.

Tepmatee and Siriphannon (2013) showed that the basal spacing of their synthesized Al-pil Mt increased from 1.24 nm to 1.69 or 1.77 nm (depending on the synthesis method used) due to the intercalation of the aluminum cations. The larger interlayer distance in the Al-pil Mt clay compared to K30 Mt is illustrated by the Al-pil clay having 5 wt% more water content compared to K30 Mt. Furthermore, the water contained in the Al-pil Mt also requires less thermal energy to evaporate than from the K30 Mt as illustrated by the steeper slope around 100°C for the Al-pil Mt (see Fig. 4). At higher temperatures, the clays still have weight loss as the water bound to the clay surface requires more thermal energy to evaporate (300°C), and dehydroxylation of the clays takes place at 500°C (Xie et al., 2001).

Literature reports three major weight loss steps for pure SPEEK: <3 wt% loss below 200°C, which is attributed to the evaporation of water from the hydrophilic polymer, a desulfonation step ($4\ SO_3H \rightarrow 4\ SO_2 + 2\ H_2O + O_2$) between 250 and 400°C and a polymer backbone degradation step above 500°C (Xing et al., 2004; Knauth et al., 2011). Fig. 4 only shows the water evaporation step and the main backbone degradation step. The desulfonation step is not observed since the membranes were in the sodium form, which hinders the proto-desulfonation of the SPEEK as demonstrated by Koziara et al. (2016).

The addition of clays to the polymer does not affect the thermal stability of the polymer itself, since the water evaporation and main backbone degradation steps are still observed. However, a higher total weight loss is observed for the composite membranes due to the presence of the highly hydrophilic clays. This increase in weight loss due to water evaporation is in the order of 0.02 residual weight for the K30 Mt and 0.075 residual weight for the Al-pil Mt. This is in accordance with the previously-made observation that the Al-pil Mt contains more water in its larger interlayer spacing than K30 Mt. However, in both cases, the amount of weight loss due to water evaporation does not show the expected increase with a higher clay loading. This is due to the highly hydrophilic samples that can absorb moisture from the atmosphere during the sample preparation and handling. It is interesting to notice that the main backbone degradation of the K30 Mt samples happens on average 25°C higher than that of SPEEK, while that increase is up to 50°C for the Al-pil Mt samples. This suggests that the addition of clays improves the thermal stability of the membranes, which is attributed to the formation of Mt-SPEEK interfaces with improved thermal stability, as reported by Chipara et al. (2008) for polypropylene-carbon nanofibers composites. In the case of the K30 Mt samples, the clay loading has a very limited effect on the extent to which the thermal stability is enhanced. For the Al-pil Mt samples, the 15 wt% clay loading shows the highest improvement in thermal stability, while the T_g results showed the maximum effect of clay on the thermal behavior at 10 wt%. This suggests that the most pronounced effect of the addition of Al-pil Mt on the thermal properties of the membrane is obtained at clay loadings between 10 and 15 wt%.

3.2. Ion exchange capacity, water uptake, and charge density

The charge density of an ion exchange membrane is important to determine its co-ion exclusion ability as well as the number of charges available for ionic transport. Figs. 5 and 6 show the IEC and the water uptake of the composite membranes, respectively.

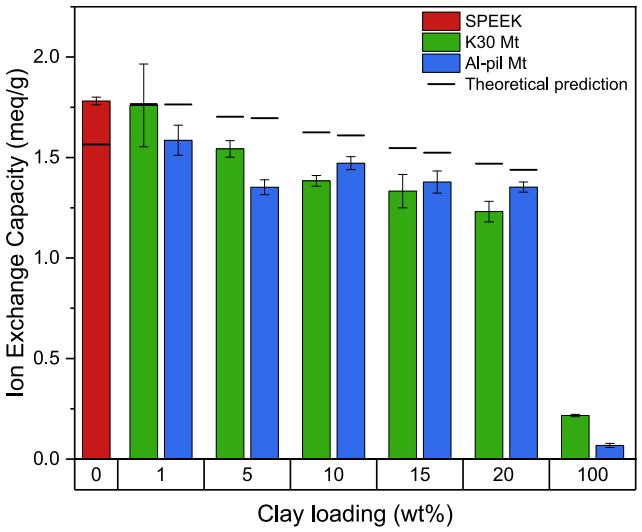

Fig. 5. Ion exchange capacity of native SPEEK and the various composite membranes. The theoretical IEC of pure SPEEK is the IEC provided by the SPEEK provider (FumaTech). The theoretical predictions of the clay composite membranes are computed by taking the relative contribution of the SPEEK polymer and the clays based on the experimental values.

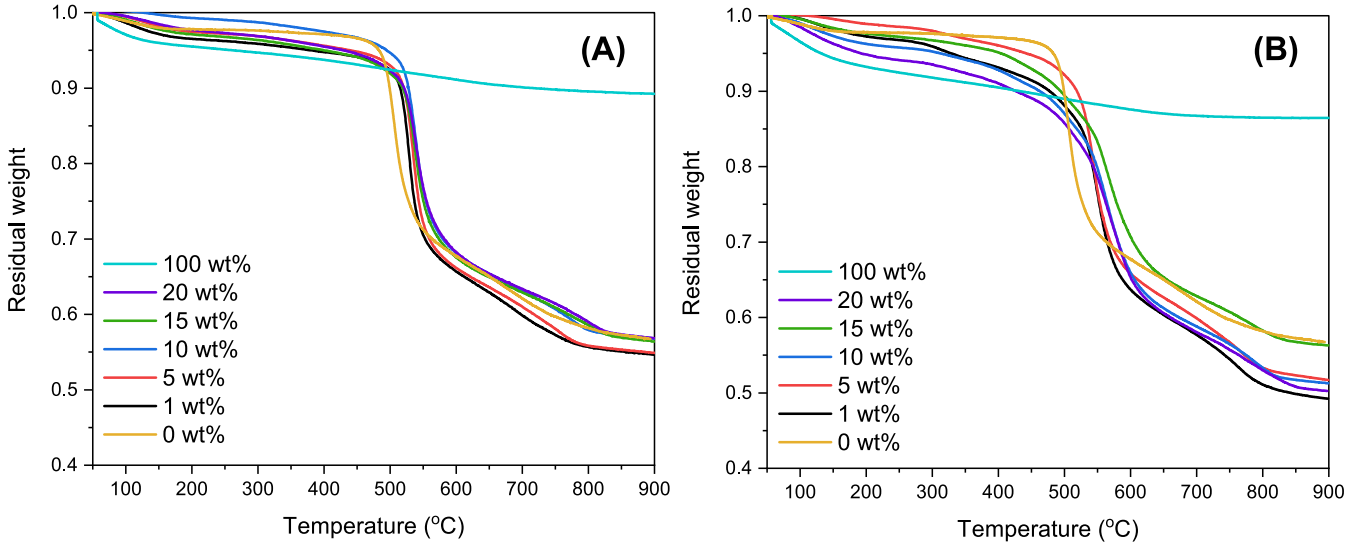

Fig. 4. TGA of the various composite membranes. The weight percentages refer to the clay loading fractions, with 100% being the powdered clays as purchased, 0 wt % being the cast 100 wt% SPEEK membrane, and the other percentages referring to the composite membranes. Figure (A) corresponds to the K30 Mt composite membranes and Figure (B) to the Al-pil Mt composite membranes.

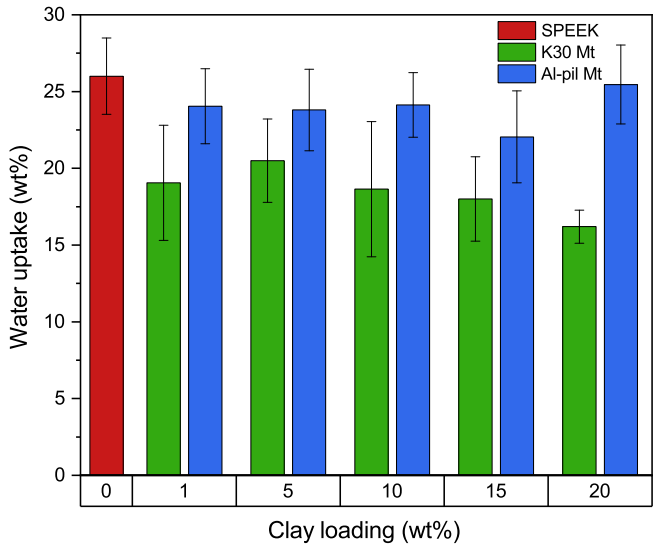

Fig. 6. Water uptake of SPEEK and the various composite membranes.

The experimentally determined SPEEK IEC is 1.78 meq/g, which is larger than the value provided by the manufacturer based on nuclear magnetic resonance spectroscopy (1.565 meq/g). This overestimation is attributed to a small amount of remaining sorbed protons in the membrane, even after thorough washing. The measured IEC of the clays is much lower than that of the polymer, i.e., 0.291 meq/g for K30 Mt and 0.115 meq/g for Al-pil Mt, respectively. The obtained IEC value for K30 Mt is three times lower than the typical values reported for Na—Mt (Hojiyev et al., 2017; Król-Morkisz and Pielichowska, 2019). The lower K30 Mt IEC is caused by the acid treatment of the clay by the manufacturer to increase the surface area for catalysis purposes, which leads to the reduction of the ion exchange capacity (Flessner et al., 2001). Nonetheless, the value obtained for the K30 Mt has a similar order of magnitude as the value reported by Rashidzadeh and Olad (2014) and Ngoh and Nawi (2016). The IEC of the Al-pil Mt is lower than the typical value for Na—Mt since the formation of each aluminum oxide pillar blocks seven permanent charges of the clay platelet surface (Gil et al., 2000; Melo et al., 2021).

As a result of the low IEC of the clays, the IEC of the composite membrane decreases with increasing clay loading. In addition, the measured IEC is also lower than the predicted theoretical IEC, indicating that the accessibility of some charged groups to cations is hindered. This is either due to the barrier effect of the clays which reduces the accessibility of some charged groups for ions, or a direct result of the clay-polymer interaction as evidenced by the FT-IR in Fig. 3, and as suggested by Hosseini et al. (2016). The measured IEC is 0.13 meq/g and 0.34 meq/g lower than the theoretically expected value for the 1 wt% and 5 wt% Al-pil Mt samples, respectively. This reduction in ion exchange group accessibility is less pronounced for exfoliated K30 Mt structures obtained at 1 and 5 wt% K30 Mt, which show no loss in IEC and a reduction of 0.16 meq/g, respectively. This is because the polymer chains are entrapped in the clay interlayers in intercalated structures of Al-pil Mt, which largely reduces their accessibility to ions. While the decrease in IEC with increasing clay concentration is steady for the K30 Mt, the Al-pil Mt IEC data is divided into two parts: the IEC increases from 1.35 meq/g to 1.47 meq/g between 5 and 10 wt% Al-pil Mt. Based on the EDS and the T_g data, the clay and polymer domains become more segregated above 10 wt% Al-pil Mt, and the number of polymer-clay interactions relative to the added amount of clay added decreases. Therefore, relatively more polymer ion exchange groups are available to contribute to the membrane IEC compared to the amount of clay added.

Remarkably, the water uptake of each kind of composite membrane is relatively independent of the respective clay loading (see Fig. 6). This does not follow the correlation found by Namdari et al. (2017) and Radmanesh et al. (2019), where the water uptake of the membranes followed the same trend as the IEC as a function of the added clay fraction. Despite a lower IEC with an increasing clay loading fraction as shown in Fig. 5, the K30 and Al-pil Mt are hydrophilic additives as evidenced by the TGA results (Fig. 4). The hydrophilicity of the clays compensates for the lower osmotic swelling of the membrane expected from the lower IEC. The water uptake of the membrane decreases from 26.0 wt% to an average of 18.5 wt% with the addition of K30 Mt, while it remains relatively unchanged by the addition of Al-pil Mt (23.7 wt%). As suggested by the TGA results, this is attributed to the larger hydrophilic interlayer spacings between the clay platelets of Al-pil Mt. These create small plasticizing free volume elements in the membrane that can be filled with water, while the strong SPEEK-K30 Mt interactions and the filling of free volume elements by exfoliated K30 platelets prevent excessive membrane swelling and even reduce the swelling of the native SPEEK polymer.

Based on the water uptake (WU in wt%) and IEC (in meq/g), the membrane charge density (ρ in meq/ g wet membrane) can be calculated using the following formula (Hugo et al., 2018):

$$\rho = \frac{\text{IEC}}{\text{WU}} \bullet 100\% \tag{6}$$

The results are shown in Fig. 7. The 1 wt% K30 Mt composite has the highest charge density (9.2 meq/g wet membrane) of all the membranes. This is as expected due to the highest IEC (1.76 meq/g) and the low water uptake (19.0 wt%) of this membrane. The other K30 Mt composites have a higher charge density (7.5 meq/g wet membrane on average) than the SPEEK membranes (6.9 meq/g wet membrane) thanks to the lower water uptake of the K30 Mt composites, which compensates for their lower IEC. On the other hand, the Al-pil Mt composites have an average charge density of 6.0 meq/g wet membrane, which is lower than the reference SPEEK membrane, resulting from both their lower IEC and their similar water uptake. Therefore, it is expected that the 1 wt% K30 composite membranes will have the best ability to selectively transport sodium ions over chloride ions, as will be discussed in the following section.

3.3. *Membrane permselectivity*

The permselectivities of the lab-made composite membranes are reported in Fig. 8. The shape of the graph is resemblant to that reporting

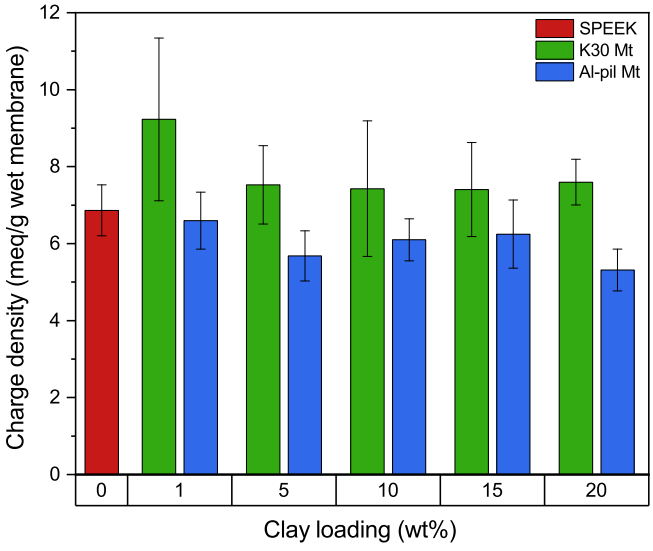

Fig. 7. Charge density of SPEEK and the composite membranes as a function of the clay loading.

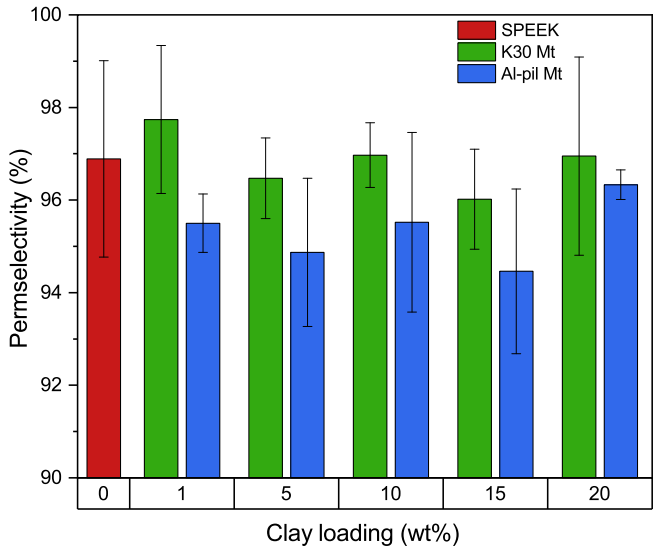

Fig. 8. Permselectivity of SPEEK and the various clay composite membranes as a function of the clay loading.

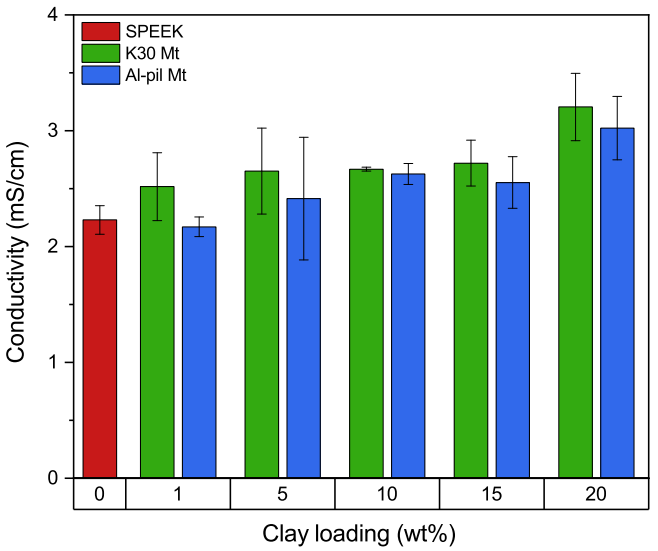

Fig. 9. Conductivity of SPEEK and the various clay composite membranes as a function of the clay loading.

the charge density in Fig. 7. This is due to the direct effect of charge density on selectivity. A lower charge density leads to a lower partitioning between the membrane and the solution, resulting in a higher co-ion concentration and a lower counter-ion concentration in the membrane (Fan et al., 2020; Kingsbury and Coronell, 2021). Since the Al-pil Mt composites have a charge density lower by 1.2 to 2.6 meq/g wet membrane than that of the K30 composites, their permselectivity is lower by 1.4 to 2% relative to the K30 Mt samples for each clay loading, except the 20 wt% composite membranes, for which the difference is only of 0.6 wt%.

However, there are some small divergences between the charge density and the permselectivity data as three small local maxima are observed at 1, 10, and 20 wt% K30 Mt while this is only observed at 10 and 20 wt% Al-pil Mt. This trend is similar to that reported by Shukla and Thakur (2010) for the conductivity of solid polymer electrolytes based on poly(methyl methacrylate) and modified Mt clays. The authors attributed this trend to different interactions between the polymer, mobile lithium ions, and clays at increasing clay loading, going from an exfoliated composite structure to an intercalated structure.

The best permselectivity is measured for the 1 wt% K30 Mt (97.7%) due to the larger charge density of this membrane, but also to a better repartition of the exfoliated K30 Mt clay platelets (see Fig. 1). The reduction of the polymer chains' mobility and the filling of the membrane free volume elements by the exfoliated K30 platelets (Table 1) prevent co-ion leakage over the membrane. This cannot be achieved with Al-pil Mt due to the inorganic crosslinks between the clay platelets. It is believed that this well-exfoliated structure acts as a barrier and increases the tortuosity of the co-ion diffusion path (Chang et al., 2003; Gaowen and Zhentao, 2005; Gosalawit et al., 2008). The local maximum observed at 10 wt% corresponds to the clay weight fraction at which there is the most clay-polymer interaction as seen with the T_g results. This clay-polymer interaction leads to the dissociation of the sodium ions coordinated by the polymer backbone, hence increasing the number of free counter-ions in the membrane, favorably affecting the membrane permselectivity (Shukla and Thakur, 2010). Finally, the higher permselectivity at 20 wt% is attributed to the formation of clay aggregates with reduced co-ion permeability as the negatively charged platelets both repel co-ions and increase their pathway tortuosity.

3.4. Membrane conductivity and sodium ion diffusion

Finally, the conductivity of the composite membranes is reported in Fig. 9.

The membrane conductivity increases with an increasing clay loading fraction, reaching up to 1.4 times that of the native SPEEK membrane for the 20 wt% K30 Mt. This is due to the formation of straight percolating sodium diffusion pathways along the 2D clay surfaces and within the straight hydrophilic interlayers between clay platelets. The higher the clay loading, the higher the amount of such straight channels, thus the higher the conductivity. In addition to the reduction in tortuosity, the membrane thickness fraction that consists of clay aggregates increases at higher clay loading fractions as shown in the EDS images (see Fig. 1). This causes an associated relative reduction of the dense polymer layer thickness, which also leads to a higher conductivity. Therefore, to achieve high conductivity and lower the ohmic losses of an electrochemical cell, having the highest clay loading (20 wt %) is the best. This finding is opposite to that of Gaowen and Zhentao (2005), who reported a decrease in proton conductivity with increasing Mt loading. This is a result of their functionalization of the Mt with hexadecyltrimethylammonium chloride, which rendered the clays non-ionic conductive, resulting in longer proton diffusion pathways (Gaowen and Zhentao, 2005).

The higher ionic mobility in composite membranes is well displayed by the diffusion coefficients (see Fig. 10) which were computed using the Nernst-Einstein equation:

$$D_{Na^+} = \frac{\sigma\, k\, T}{e^2 N} \tag{7}$$

where D_{Na^+} is the sodium ion diffusion coefficient (m^2/s), σ is the experimental value of the membrane conductivity (S/m), k is Boltzmann constant (J/K), T the temperature (K), e the elemental charge (C), N the number density of sodium ions (number per m^3), computed from the membrane charge density.

Fig. 10 shows that the diffusion coefficient increases by a factor of 1.2 between 1 and 5 wt%, which indicates the first threshold for the increase in diffusion coefficient, which is correlated with the formation of clay aggregates. In those regions, the clay platelets are segregated from the polymer and retain their initial platelet organization in which the sodium ions experience less tortuosity than in the polymer matrix. As the clay loading in the membrane increases from 0 to 20 wt%, the fraction of membrane area that contains clay aggregates increases, which explains the increase in diffusion coefficient at higher clay loadings, reaching 11.2×10^{-12} m^2/s for 20 wt% K30 Mt and 15.2×10^{-12} m^2/s for 20 wt% Al-pil Mt.

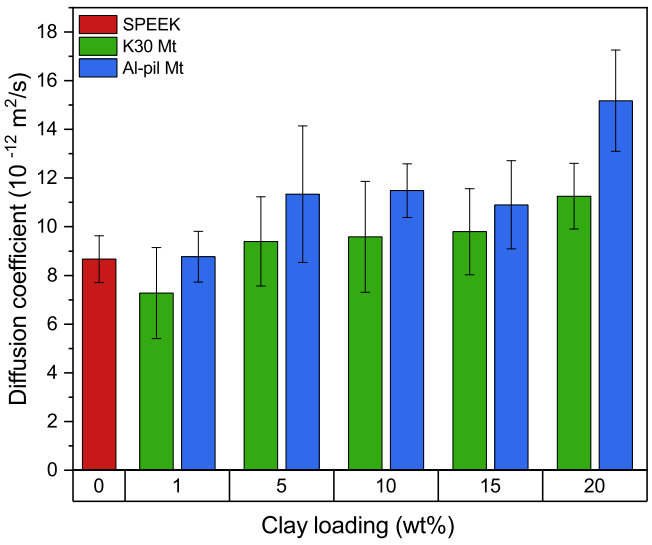

Fig. 10. Computed sodium diffusion coefficient using the Nernst Einstein equation as a function of the clay loading.

The fact that the diffusion coefficient is larger in the Al-pil composite membranes by 1.1×10^{-12} to 3.9×10^{-12} m^2/s compared to the K30 Mt membranes is attributed to the higher water uptake of these membranes. Despite their lower charge density, the Al-pil Mt clays have a larger interlayer spacing, creating a hydrated volume in which the ions have greater mobility as computed by Greathouse et al. (2016). This shows that the addition of non-compatibilized K30 and Al-pil Mt clays with large hydrated interlayer spacing is a promising strategy to increase the ion mobility in CEMs. By tuning the charge density and the interlayer spacing of the clays as well as the polymer-clay composite morphology, membranes with tunable conductivities and permselectivities can be obtained. For electrochemical applications, membranes with low resistance and high permselectivity are desirable as they contribute the least to the Ohmic losses of a system while preventing the undesired crossover of ions. From the results presented in Fig. 8 through Fig. 10, it appears that the membranes with the highest clay loading (20 wt%) are the most suitable since they have the lowest resistance while their permselectivity remains at 96.9% and 96.3% for the K30 Mt and Al-pil Mt, respectively.

3.5. Membrane performance in a concentration gradient battery

To illustrate the advantages of such composite membranes in a salinity gradient flow battery, the performance of the SPEEK membrane and the 20 wt% K30 and Al-pil Mt composite membranes in a lab-scale concentration gradient battery was evaluated, since these two membranes showed the most improvement in conductivity.

The average coulombic, voltaic, and round-trip efficiencies are reported in Table 2.

All the experiments have a coulombic efficiency of 100.0% since the charge and the discharge steps were set at the same current for the same amount of time. However, both the voltaic efficiency as well as the round-trip efficiency of the clay composite membranes outperform that of the native SPEEK membrane. The voltaic efficiency and the round-trip efficiency are the best for the 20 wt% K30 Mt composite membrane (92.7%), followed by the 20 wt% Al-pil Mt (86.6%) and the SPEEK membrane (82.7%). This result is in line with the conductivity results shown in Fig. 10. When a membrane has a higher conductivity, its resistivity is lower, which lowers the membrane's contribution to the ohmic overpotential (Vermaas et al., 2012). This lower overpotential directly improves the voltaic efficiency of the cell, and thus, its round-trip efficiency as well. This suggests that the addition of non-compatibilized clays to a polymer membrane is a promising method for improving the membrane conductivity and thus, the voltaic and round-trip efficiency of the system.

Table 2
Thickness, coulombic, voltaic, and round-trip efficiencies of the SPEEK, 20 wt% K30 Mt and 20 wt% Al-pil Mt composite membranes.

	SPEEK	20 wt% K30 Mt	20 wt% Al-pil Mt
Thickness (μm)	51	71	66
Coulombic efficiency	100.0 ± 0.0%	100.0 ± 0.0%	100.0 ± 0.0%
Voltaic efficiency	82.7 ± 2.2%	92.7 ± 2.8%	86.6 ± 3.1%
Round-trip efficiency	82.7 ± 2.2%	92.7 ± 2.8%	86.6 ± 3.1%

4. Conclusion

Clay-polymer composite cation exchange membranes based on 1 to 20 wt% K30 Mt and Al-pil Mt and SPEEK were made. The lack of compatibilizer creates micro composite membranes containing clay aggregates in which the clays retain their stacked platelet morphology when the clay percentage is above 5 wt%. The straight hydrophilic channels between the clay platelets enable sodium ions to migrate through the membrane with a reduced tortuosity, thereby increasing their diffusion coefficient in the membrane with increasing clay loading. The sodium diffusion coefficient of the 20 wt% Al-pil membrane is 15.2×10^{-12} m^2/s, which is higher than that of the 20 wt% K30 Mt (11.3×10^{-12} m^2/s), with both membranes showing a significant improvement compared to the SPEEK membrane (8.6×10^{-12} m^2/s). The increase in sodium diffusion is more pronounced in the case of Al-pil Mt than K30 Mt as the mobile cations have a greater mobility in the more hydrated interlayer of pillared clays. In the case of Al-pil Mt, the permselectivity was slightly lower than that of a pure SPEEK matrix by no more than 3% due to the large hydrophilic interlayer spaces of the pillared clay that favor co-ion transport. On the other hand, the 1, 10, and 20 wt% K30 Mt have an improved permselectivity thanks to the barrier effect of the clays towards co-ions and the polymer-clay interactions in the case of the 10 wt% K30 Mt composite membrane. From the conductivity and permselectivity results, it was concluded that the best membranes are those with 20 wt% clay loading since the increase in conductivity is the highest while the permselectivity remains similar to that of the pure SPEEK membrane. In general, the incorporation of non-compatibilized K30 Mt or Al-pil Mt clay into a SPEEK matrix is a facile method to improve the conductivity of cation exchange membranes with limited permselectivity loss. This has the potential to positively influence the voltaic and round-trip efficiency of aqueous redox flow batteries. This is demonstrated in a salt concentration gradient battery, where the cell with the 20 wt% K30 Mt membrane has a 10.0% improvement of the voltaic efficiency compared to the reference cell with a 100% SPEEK membrane. This improvement was only 3.9% for the 20 wt% Al-pil composite membrane.

5. Challenges and future prospective

This work has shown that the addition of non-compatibilized K30 Mt and Al-pil Mt to a SPEEK matrix is a promising method for improving the cation exchange membrane conductivity while maintaining permselectivities above 94.4%. Therefore, these membranes are attractive for electrochemical applications where there is an interest in lowering the membrane's contribution to the Ohmic losses of a system.

The membranes were able to withstand short experiments in an electrodialysis cell. Nonetheless, the mechanical stability of these membranes in more challenging electrochemical systems needs to be tested and addressed. Even though the addition of clays enhances the thermal stability of the clays, it is expected that the clay-polymer interfaces are mechanically weak regions that can crack under challenging operating conditions. Furthermore, some of the electrochemical applications in the electrochemical require acidic operating conditions. While SPEEK has been reported for such applications, it is expected that the

clays are not chemically stable as highly acidic environments can cause the leaching of metal ions from the clays. Therefore, it is necessary to look into the improvement of the membrane's stability in acidic media, for example, by adding a protective layer around the clays or on the membrane surface.

Credit authorship contribution statement

Nadia Boulif contributed to the conceptualization, methodology, investigation, data curation and writing. **Renate Evers** contributed to the investigation and data curation. **Menno Houben** contributed to the writing - review & editing. **Zandrie Borneman** and **Kitty Nijmeijer** contributed to the funding acquisition, resources, conceptualization, writing and project administration.

Declaration of Competing Interest

The authors declare that they have no known competing financial interests or personal relationships that could have appeared to influence the work reported in this paper.

Data availability

Data will be made available on request.

Acknowledgment

This work was supported by the Dutch Research Council (NWO) [grant number 17621]. The authors would like to thank Joey Kloos and Niki Joosten for their help with the DSC measurements.

Appendix A. Supplementary data

Supplementary data to this article can be found online at https://doi.org/10.1016/j.clay.2023.107136.

References

Abbasi, S., Forner-Cuenca, A., Kout, W., Nijmeijer, K., Borneman, Z., 2021. Low-cost wire-electrospun sulfonated poly(ether ether ketone)/poly(vinylidene fluoride) blend membranes for hydrogen-bromine flow batteries. J. Membr. Sci. 628, 119258. https://doi.org/10.1016/j.memsci.2021.119258.

Al-Dhubhani, E., Pärnamäe, R., Post, J.W., Saakes, M., Tedesco, M., 2021. Performance of five commercial bipolar membranes under forward and reverse bias conditions for acid-base flow battery applications. J. Membr. Sci. 640, 119748. https://doi.org/10.1016/j.memsci.2021.119748.

Bhattacharya, M., 2016. Polymer nanocomposites—a comparison between carbon nanotubes, graphene, and clay as nanofillers. Materials 9, 262. https://doi.org/10.3390/ma9040262.

Bourg, I.C., Sposito, G., 2010. Connecting the molecular scale to the continuum scale for diffusion processes in smectite-rich porous media. Environ. Sci. Technol. 44, 2085–2091. https://doi.org/10.1021/es903645a.

Chang, J.-H., Park, J.H., Park, G.-G., Kim, C.-S., Park, O.O., 2003. Proton-conducting composite membranes derived from sulfonated hydrocarbon and inorganic materials. J. Power Sources 124, 18–25. https://doi.org/10.1016/S0378-7753(03)00605-0.

Charradi, K., Ahmed, Z., Aranda, P., Chtourou, R., 2019. Silica/montmorillonite nanoarchitectures and layered double hydroxide-SPEEK based composite membranes for fuel cells applications. Appl. Clay Sci. 174, 77–85. https://doi.org/10.1016/j.clay.2019.03.027.

Chipara, Magdalena, Lozano, K., Hernandez, A., Chipara, Mircea, 2008. TGA analysis of polypropylene–carbon nanofibers composites. Polym. Degrad. Stab. 93, 871–876. https://doi.org/10.1016/j.polymdegradstab. 2008.01.001.

DeFelice, J., Lipson, J.E.G., 2021. The influence of additives on polymer matrix mobility and the glass transition. Soft Matter 17, 376–387. https://doi.org/10.1039/D0SM01634A.

Doğan, H., Inan, T.Y., Koral, M., Kaya, M., 2011. Organo-montmorillonites and sulfonated PEEK nanocomposite membranes for fuel cell applications. Appl. Clay Sci. 52, 285–294. https://doi.org/10.1016/j.clay.2011.03.007.

Fan, H., Yip, N.Y., 2019. Elucidating conductivity-permselectivity tradeoffs in electrodialysis and reverse electrodialysis by structure-property analysis of ion-exchange membranes. J. Membr. Sci. 573, 668–681. https://doi.org/10.1016/j.memsci.2018.11.045.

Fan, H., Huang, Y., Yip, N.Y., 2020. Advancing the conductivity-permselectivity tradeoff of electrodialysis ion-exchange membranes with sulfonated CNT nanocomposites. J. Membr. Sci. 610, 118259. https://doi.org/10.1016/j.memsci.2020.118259.

Flessner, U., Jones, D.J., Rozière, J., Zajac, J., Storaro, L., Lenarda, M., Pavan, M., Jiménez-López, A., Rodríguez-Castellón, E., Trombetta, M., Busca, G., 2001. A study of the surface acidity of acid-treated montmorillonite clay catalysts. J. Mol. Catal. A Chem. 168, 247–256. https://doi.org/10.1016/S1381-1169(00)00540-9.

Gaowen, Z., Zhentao, Z., 2005. Organic/inorganic composite membranes for application in DMFC. J. Membr. Sci. 261, 107–113. https://doi.org/10.1016/j.memsci.2005.03.036.

Ghasemi, M., Daud, W.R.W., Ismail, A.F., Jafari, Y., Ismail, M., Mayahi, A., Othman, J., 2013. Simultaneous wastewater treatment and electricity generation by microbial fuel cell: performance comparison and cost investigation of using Nafion 117 and SPEEK as separators. Desalination 325, 1–6. https://doi.org/10.1016/j.desal.2013.06.013.

Gil, A., Vicente, M.A., Gandía, L.M., 2000. Main factors controlling the texture of zirconia and alumina pillared clays. Microporous Mesoporous Mater. 34, 115–125. https://doi.org/10.1016/S1387-1811(99)00166-3.

Gosalawit, R., Chirachanchai, S., Shishatskiy, S., Nunes, S.P., 2008. Sulfonated montmorillonite/sulfonated poly(ether ether ketone) (SMt/SPEEK) nanocomposite membrane for direct methanol fuel cells (DMFCs). J. Membr. Sci. 323, 337–346. https://doi.org/10.1016/j.memsci.2008.06.038.

Greathouse, J.A., Cygan, R.T., Fredrich, J.T., Jerauld, G.R., 2016. Molecular dynamics simulation of diffusion and electrical conductivity in montmorillonite interlayers. J. Phys. Chem. C 120, 1640–1649. https://doi.org/10.1021/acs.jpcc.5b10851.

Guggenheim, E.A., 1954. The diffusion coefficient of sodium chloride. Trans. Faraday Soc. 50, 1048. https://doi.org/10.1039/tf9545001048.

Guler, E., Nijmeijer, K., 2018. Reverse electrodialysis for salinity gradient power generation: challenges and future perspectives. JMSR 4. https://doi.org/10.22079/jmsr.2018.86747.1193.

Güler, E., Elizen, R., Vermaas, D.A., Saakes, M., Nijmeijer, K., 2013. Performance-determining membrane properties in reverse electrodialysis. J. Membr. Sci. 446, 266–276. https://doi.org/10.1016/j.memsci.2013.06.045.

Hojiyev, R., Ulcay, Y., Hojamberdiev, M., Çelik, M.S., Carty, W.M., 2017. Hydrophobicity and polymer compatibility of POSS-modified Wyoming Na-montmorillonite for developing polymer-clay nanocomposites. J. Colloid Interface Sci. 497, 393–401. https://doi.org/10.1016/j.jcis.2017.03.034.

Hosseini, S.M., Seidypoor, A., Nemati, M., Madaeni, S.S., Parvizian, F., Salehi, E., 2016. Mixed matrix heterogeneous cation exchange membrane filled with clay nanoparticles: membranes' fabrication and characterization in desalination process. J. Water Reuse Desalin. 6, 290–300. https://doi.org/10.2166/wrd.2015.064.

Hugo, Y.A., 2020. Membrane Development for Large-Scale Hydrogen-Bromine Flow Batteries. Technische Universiteit Eindhoven.

Hugo, Y.A., Kout, W., Sikkema, F., Borneman, Z., Nijmeijer, K., 2018. Performance mapping of cation exchange membranes for hydrogen-bromine flow batteries for energy storage. J. Membr. Sci. 566, 406–414. https://doi.org/10.1016/j.memsci.2018.09.006.

Kingsbury, R.S., Coronell, O., 2021. Modeling and validation of concentration dependence of ion exchange membrane permselectivity: significance of convection and Manning's counter-ion condensation theory. J. Membr. Sci. 620, 118411. https://doi.org/10.1016/j.memsci.2020.118411.

Kingsbury, R.S., Flotron, S., Zhu, S., Call, D.F., Coronell, O., 2018. Junction potentials bias measurements of ion exchange membrane permselectivity. Environ. Sci. Technol. 52, 4929–4936. https://doi.org/10.1021/acs.est.7b05317.

Knauth, P., Hou, H., Bloch, E., Sgreccia, E., Di Vona, M.L., 2011. Thermogravimetric analysis of SPEEK membranes: thermal stability, degree of sulfonation and cross-linking reaction. J. Anal. Appl. Pyrolysis 92, 361–365. https://doi.org/10.1016/j.jaap.2011.07.012.

Koziara, B.T., Kappert, E.J., Ogieglo, W., Nijmeijer, K., Hempenius, M.A., Benes, N.E., 2016. Thermal stability of sulfonated poly(ether ether ketone) films: on the role of protodesulfonation: thermal stability of sulfonated poly(ether ether ketone)…. Macromol. Mater. Eng. 301, 71–80. https://doi.org/10.1002/mame.201500075.

Kreuer, K.D., 2001. On the development of proton conducting polymer membranes for hydrogen and methanol fuel cells. J. Membr. Sci. 185, 29–39. https://doi.org/10.1016/S0376-7388(00)00632-3.

Krishnan, P., Park, J.-S., Kim, C.-S., 2006. Preparation of proton-conducting sulfonated poly(ether ether ketone)/boron phosphate composite membranes by an in situ sol–gel process. J. Membr. Sci. 279, 220–229. https://doi.org/10.1016/j.memsci.2005.12.010.

Król-Morkisz, K., Pielichowska, K., 2019. Thermal decomposition of polymer nanocomposites with functionalized nanoparticles. In: Polymer Composites with Functionalized Nanoparticles. Elsevier, pp. 405–435. https://doi.org/10.1016/B978-0-12-814064-2.00013-5.

Kumar, R., Mamlouk, M., Scott, K., 2014. Sulfonated polyether ether ketone – sulfonated graphene oxide composite membranes for polymer electrolyte fuel cells. RSC Adv. 4, 617–623. https://doi.org/10.1039/C3RA42390E.

Lee, W., Kim, H., Kim, T., Chang, H., 2007. Nafion based organic/inorganic composite membrane for air-breathing direct methanol fuel cells. J. Membr. Sci. 292, 29–34. https://doi.org/10.1016/j.memsci.2006.12.051.

Li, X., Li, H., Yang, G., 2017. Electric fields within clay materials: how to affect the adsorption of metal ions. J. Colloid Interface Sci. 501, 54–59. https://doi.org/10.1016/j.jcis.2017.04.040.

Mahajan, C.V., Ganesan, V., 2010. Atomistic simulations of structure of solvated sulfonated poly(ether ether ketone) membranes and their comparisons to Nafion: I. Nanophase segregation and hydrophilic domains. J. Phys. Chem. B 114, 8357–8366. https://doi.org/10.1021/jp104078h.

Massaro, M., Cavallaro, G., Lazzara, G., Riela, S., 2020. Covalently modified nanoclays: synthesis, properties and applications. In: Clay Nanoparticles. Elsevier, pp. 305–333. https://doi.org/10.1016/B978-0-12-816783-0.00013-X.

Melo, V.F., Salata, R., Abate, G., Azevedo, A.C., Kummer, L., 2021. Characterization and manipulation of montmorillonite properties towards technological and environmental applications. Rev. Bras. Ciênc. Solo 45, e0200149. https://doi.org/10.36783/18069657rbcs20200149.

Müller, K., Bugnicourt, E., Latorre, M., Jorda, M., Echegoyen Sanz, Y., Lagaron, J., Miesbauer, O., Bianchin, A., Hankin, S., Bölz, U., Pérez, G., Jesdinszki, M., Lindner, M., Scheuerer, Z., Castelló, S., Schmid, M., 2017. Review on the processing and properties of polymer nanocomposites and nanocoatings and their applications in the packaging, automotive and solar energy fields. Nanomaterials 7, 74. https://doi.org/10.3390/nano7040074.

Muralidharan, M.N., Kumar, S.A., Thomas, S., 2008. Morphology and transport characteristics of poly(ethylene-co-vinyl acetate)/clay nanocomposites. J. Membr. Sci. 315, 147–154. https://doi.org/10.1016/j.memsci.2008.02.013.

Namdari, M., Kikhavani, T., Ashrafizadeh, S.N., 2017. Synthesis and characterization of an enhanced heterogeneous cation exchange membrane via nanoclay. Ionics 23, 1745–1758. https://doi.org/10.1007/s11581-017-2009-x.

National Institute for Public Health and the Environment, 2023. PFAS Restricition Proposal [WWW Document]. rivm.nl. URL. https://www.rivm.nl/en/pfas/pfas-restriction-proposal (accessed 3.16.22).

Ngoh, Y.S., Nawi, M.A., 2016. Fabrication and properties of an immobilized P25TiO 2 -montmorillonite bilayer system for the synergistic photocatalytic–adsorption removal of methylene blue. Mater. Res. Bull. 76, 8–21. https://doi.org/10.1016/j.materresbull.2015.11.060.

Nijmeijer, K., Metz, S., 2010. Chapter 5 salinity gradient energy. In: Sustainability Science and Engineering. Elsevier, pp. 95–139. https://doi.org/10.1016/S1871-2711(09)00205-0.

Radmanesh, F., Rijnaarts, T., Moheb, A., Sadeghi, M., de Vos, W.M., 2019. Enhanced selectivity and performance of heterogeneous cation exchange membranes through addition of sulfonated and protonated montmorillonite. J. Colloid Interface Sci. 533, 658–670. https://doi.org/10.1016/j.jcis.2018.08.100.

Rashidzadeh, A., Olad, A., 2014. Slow-released NPK fertilizer encapsulated by NaAlg-g-poly(AA-co-AAm)/Mt superabsorbent nanocomposite. Carbohydr. Polym. 114, 269–278. https://doi.org/10.1016/j.carbpol.2014.08.010.

Sarapulova, Shkorkina, Mareev, Pismenskaya, Kononenko, Larchet, Dammak, Nikonenko, 2019. Transport characteristics of Fujifilm ion-exchange membranes as compared to homogeneous membranes AMX and CMX and to heterogeneous membranes MK-40 and MA-41. Membranes 9, 84. https://doi.org/10.3390/membranes9070084.

Shukla, N., Thakur, A.K., 2010. Ion transport model in exfoliated and intercalated polymer–clay nanocomposites. Solid State Ionics 181, 921–932. https://doi.org/10.1016/j.ssi.2010.05.023.

Tepmatee, P., Siriphannon, P., 2013. Effect of preparation method on structure and adsorption capacity of aluminum pillared montmorillonite. Mater. Res. Bull. 48, 4856–4866. https://doi.org/10.1016/j.materresbull.2013.06.066.

Uddin, F., 2018. Montmorillonite: an introduction to properties and utilization. In: Zoveidavianpoor, M. (Ed.), Current Topics in the Utilization of Clay in Industrial and Medical Applications. InTech. https://doi.org/10.5772/intechopen.77987.

van Egmond, W.J., Saakes, M., Porada, S., Meuwissen, T., Buisman, C.J.N., Hamelers, H. V.M., 2016. The concentration gradient flow battery as electricity storage system: technology potential and energy dissipation. J. Power Sources 325, 129–139. https://doi.org/10.1016/j.jpowsour.2016.05.130.

Vermaas, D.A., Guler, E., Saakes, M., Nijmeijer, K., 2012. Theoretical power density from salinity gradients using reverse electrodialysis. Energy Procedia 20, 170–184. https://doi.org/10.1016/j.egypro.2012.03.018.

Xie, W., Gao, Z., Liu, K., Pan, W.-P., Vaia, R., Hunter, D., Singh, A., 2001. Thermal characterization of organically modified montmorillonite. Thermochim. Acta 367–368, 339–350. https://doi.org/10.1016/S0040-6031(00)00690-0.

Xing, P., Robertson, G.P., Guiver, M.D., Mikhailenko, S.D., Wang, K., Kaliaguine, S., 2004. Synthesis and characterization of sulfonated poly(ether ether ketone) for proton exchange membranes. J. Membr. Sci. 229, 95–106. https://doi.org/10.1016/j.memsci.2003.09.019.

Xu, W.B., Zhou, Z.F., Ge, M.L., Pan, W.-P., 2004. Polyvinyl chloride/ montmorillonite nanocomposites. J. Therm. Anal. Calorim. 78, 91–99. https://doi.org/10.1023/B:JTAN.0000042157.96074.44.

Zhou, C., Tong, D., Yu, W., 2019. Smectite nanomaterials: preparation, properties, and functional applications. In: Nanomaterials from Clay Minerals. Elsevier, pp. 335–364. https://doi.org/10.1016/B978-0-12-814533-3.00007-7.